Applied Surface Science 258 (2012) 5135–5140

Contents lists available at SciVerse ScienceDirect

Applied Surface Science

journal homepage: www.elsevier.com/locate/apsusc

A novel Ir–Zr gradient coating prepared on Mo substrate by double glow plasma

Xiangna Cong, Zhaofeng Chen*, Wangping Wu, Jiang Xu, Fred Edmond Boafo

College of Material Science and Technology, Nanjing University of Aeronautics and Astronautics, Nanjing 210016, PR China

ARTICLE INFO

Article history:
Received 8 October 2011
Received in revised form
30 December 2011
Accepted 25 January 2012
Available online 2 February 2012

Keywords:
Iridium
Zirconium
Structure
Gradient coating

ABSTRACT

Ir–Zr gradient coating was obtained on the Mo substrate by double glow plasma. The structure and composition of the coatings were confirmed by SEM, AFM, XRD and EDS, respectively. The adhesion strength between the coating and the substrate was evaluated by a scratch tester. Compared with preferential growth orientation of (2 2 0) crystal plane of Ir coating, the Ir–Zr coating had a random orientation structure. The RMS roughness value of the Ir–Zr coating is 19.3 nm, which was lower than the roughness value of 45 nm for Ir coating. The Ir–Zr coating with the thickness of 5.0 μm was composed of two distinct layers. The proportion of Ir decreased gradually from the surface of the coating to the coating/substrate interface. The Zr distribution decreased slightly in the coating. The adhesive force of the Ir–Zr coating was 15 N.

1. Introduction

The refractory metal molybdenum (Mo) has a combination of properties, including exceptional strength, stiffness at high temperature, good thermal conductivity and low thermal expansion, which are useful in wide range of applications, particularly at elevated temperatures such as high temperature furnaces, rockets nozzles, jet tabs and fusion devices [1]. However, one major drawback of Mo is poor oxidation resistance at high temperatures [2,3]. In our previous study, iridium (Ir) was chosen to the coating materials on Mo substrate because of its low oxygen permeability, high melting temperature, good chemical compatibility, an effective barrier to carbon and oxygen diffusion [4,5] and good corrosion resistance [6,7]. Nevertheless, this procedure might cause serious problems such as the evaporation of the Ir when the materials are applied in high temperature environments. Some researchers [8,9] focused on the design of the coating such as multilayer coatings or doped alloy elements, which reduced the ablation rate and extended the useful time. At present, Ir-based alloys, Ir–X (X = Ti, Nb, Hf, Zr, Ta and V), have gained attention as new high-temperature materials due to their high melting point and superior oxidation resistance [10–13]. The behavior of Ir–Ta, Ir–Hf, Ir–Pt, Ir–Ni and Ir–Al coatings have been investigated [14–17]. However, few literatures concerning Ir–Zr coating have so far been published. In order to provide enhanced high temperature protection over a wide range of operating conditions, the Mo substrate could be improved by depositing the Ir–Zr coating based on the outstanding characteristics of Zr, such as exceptional strength, stiffness at high temperature and excellent corrosion resistance. In addition, gradient coating can be used to reduce stress concentrations at the intersection between the interface and the surface, thereby limiting the stresses at critical locations and thus suppressing the onset of damage or cracking [18,19]. Therefore, the gradient structure of Zr distribution in the Ir coating cannot only avoid the evaporation of the Ir, but also improve the distribution of stress.

Double glow plasma technique could be looked as a kind of physical vapor deposition, which could apply almost all solid metallic elements to realize surface alloying of the metallic substrates. The general advantages of this technique include low cost, high deposition rate, good coating uniformity, controllability of coating thickness and strong adhesion to the complex shaped substrates [20,21]. This technique can be used to produce the coatings with different composition ratio of coating elements in a controlled manner with simple operating procedures. In this paper, a design for gradient Ir–Zr coating was fabricated on Mo substrate by double glow plasma. The structure and adhesive properties of the coating were investigated.

2. Experiment

2.1. Preparation of the coating

A detailed description of double glow plasma device was reported in detail elsewhere [22,23]. The surface alloying

* Corresponding author.
E-mail address: zhaofeng_chen@163.com (Z. Chen).

0169-4332/$ – see front matter © 2012 Elsevier B.V. All rights reserved.
doi:10.1016/j.apsusc.2012.01.149

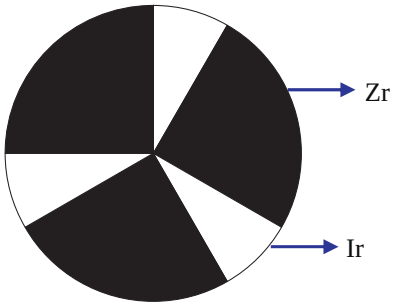

Fig. 1. Schematic diagram of the Ir–Zr target.

experiment was performed in a double glow plasma surface alloying device, in which the low temperature plasma was produced by a glow discharge process in a vacuum sputtering chamber. Three electrodes were designed in the chamber: one anode and two negatively charged members. The work piece was positioned at the cathode, and the source electrode was where the desired element was located. Some Mo plates (⌀40 mm × 3 mm) were used as the substrate materials. The substrates were polished with 1000-grit emery paper and cleaned ultrasonically in ethanol for 0.5 h before deposition. The substrates were then dried for 1 h at 353 K in order to remove the ethanol from the substrates. An alloy plate consisting of the Ir and Zr elements (Fig. 1) was used as the target which was obtained by glow plasma device. In the preparation process of the alloy plate, the Ir plate (purity: 99.95%, ⌀50 mm × 3.5 mm), segmental covered with alumina ceramic plates at equal distances, was used as the substrate, and the Zr wire (purity: 99.5%, ⌀1.5 mm × 500 mm) was the target. Since the sputtering rate of Zr was lower than that of Ir, a ratio of surface area (the half cylindrical area) of Zr to surface area of Ir of 5:1 was chosen. Argon was used as the working gas. The deposition conditions were: base pressure 4×10^{-4} Pa, target bias voltage −850 V, substrate bias voltage −300 V, substrate temperature 1073–1123 K, working gas pressure 30 Pa, target-substrate spacing 15 mm, and deposition time 2 h.

2.2. Characterization of the coating

The phase identification and crystal size of the coating were determined by X-ray diffraction (XRD, Bruker D8 Advanced) using Ni-filtered Cu Kα radiation at a scanning rate of 4°/min and scanning from 10° to 90° of 2θ. The chemical composition of the coating was examined by energy dispersive spectroscopy (EDS, Genesis 2000 XMS 60). The microstructure and morphology of the coating were observed by scanning electron microscopy (SEM, FEI CO, Quanta200). The root mean square (RMS) roughness of the coating was measured by atomic force microscopy (AFM, CSPM4000).

2.3. Adhesive property of the coating

The adhesion of the coating to the substrate was evaluated by a scratch tester (WS-2005) using a diamond stylus (120° cone with a 0.2 mm diameter tip) under continuously increasing load. The loading rate was set at 25 N/min and the specimen table speed was 4 mm/min. The test was terminated at the maximum load of 100 N.

3. Results and discussion

3.1. Structure

Fig. 2 displays the XRD patterns of the Ir coating and the Ir–Zr coating on Mo substrate. In Fig. 2a, the Ir coating had three diffraction peaks: (1 1 1), (2 0 0) and (2 2 0). The degree of preferred orientation of the coating was estimated from X-ray peak-intensity

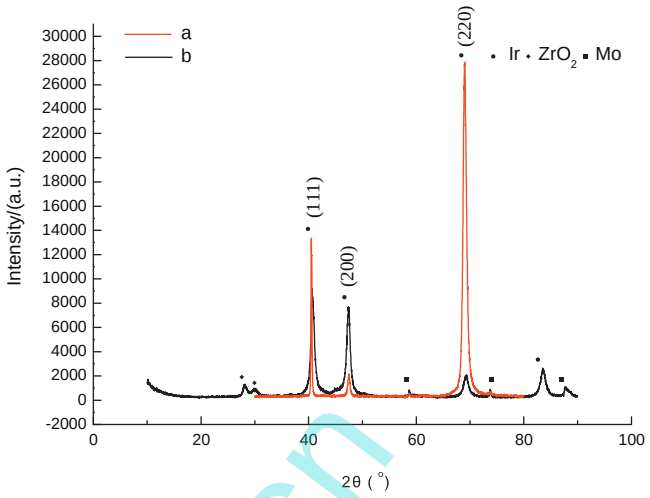

Fig. 2. XRD patterns of the Ir coating and the Ir–Zr coating.

ratios of (2 0 0) and (1 1 1) planes, as well as (2 2 0) and (1 1 1) planes (i.e., I_{200}/I_{111} and I_{220}/I_{111}). For randomly oriented Ir powder sample JCPDS (46-1044) [24], the values I_{200}/I_{111} and I_{220}/I_{111} were 0.55 and 0.42. As illustrated in the Ir coating, the values I_{200}/I_{111} and I_{220}/I_{111} were 0.17 and 2.17. The data indicated that the Ir coating had a preferred (2 2 0) orientation due to the initial nuclei with preferred growth on the surface of the substrate. The nucleation process could play an important role in determining the distribution of orientations in the resulting coating. In general, the orientation of the Ir coating by sputtering or chemical vapor deposition is (1 1 1) crystal plane. The (1 1 1) orientation is favored most likely because the (1 1 1) crystal plane in face-centered cubic (fcc) structure was closely packed with the lowest surface energy [25,26]. However, the values I_{200}/I_{111} and I_{220}/I_{111} for Ir–Zr coating (Fig. 2b) were 0.85 and 0.23, implying a random orientation. Compared with the XRD pattern of the Ir coating, the (1 1 1), (2 0 0) diffraction peaks of the Ir–Zr coating became wide and (1 1 1), (2 2 0) peak became weak. The broadening of the peak was attributable to the decrease of grain size. Further, we would need to more accurately assess the grain sizes by TEM investigation. It was found the formation of ZrO_2 was might be attributed to the reaction between Zr and O_2. The Mo was also observed in the XRD pattern which might be due to the thin Ir–Zr coating.

3.2. Morphology and composition

Fig. 3 shows the AFM images of the Ir–Zr coating. Fig. 3a shows the three-dimensional tapping mode AFM image over a 2.98 μm × 2.98 μm region of the surface morphology of the Ir–Zr coating. The surface of the Ir–Zr coating is composed of hillocks due to the shadowing effects. High points on the surface received more atoms than low points, and then hillocks and valleys developed. The RMS roughness value of the Ir–Zr coating is 19.3 nm, which was lower than the roughness of 45 nm for Ir coating [27]. Gong et al. [28] reported that the surface roughness and crystalline size of the Ir film by pulsed laser deposition increased with the increasing substrate temperature. However, deposition conditions were the same for both Ir–Zr coating and the Ir coating, the influence of experimental parameters such as the substrate temperature was neglected. It can be included that the decrease of the roughness of the Ir–Zr coating was due to the effect of the additional Zr. On the other hand, the formation of ZrO_2 phase might inhibit the grains growth of the coating. Gelfond et al. [29] suggested that the introduction of the oxide phase in the Ir coating halved the Ir crystallite size. It can be inferred that the formation of ZrO_2 phase could made

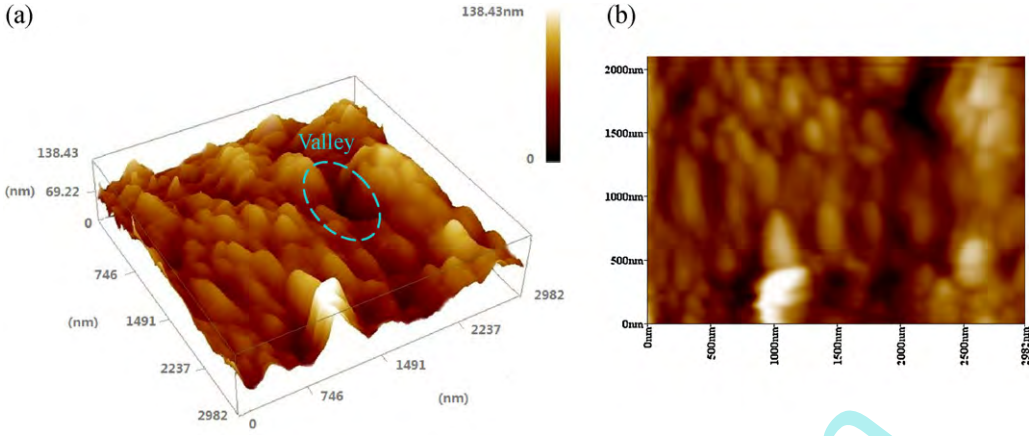

Fig. 3. AFM images of the coating: (a) 3D AFM image and (b) 2D AFM image.

the grain refining. From Fig. 3b, the grain size of the coating was about 100 nm. The grains of sub-micrometer size could be ascribed to the high substrate temperature, which enabled the thermodynamically favored grains to grow in size. It can be seen that the Ir–Zr coating was generally dense and homogeneous.

Fig. 4 shows the SEM micrographs of the surfaces of the Ir–Zr coating and Ir coating. The surface of the Ir–Zr coating was dense and uniform (Fig. 4a). The average size of grains was about 90–100 nm. Some horizontal textures appeared on the surface due to the surface treatment of the Mo substrate before the deposition. No microcracks were observed on the surface of the coating. It was found from Fig. 4b that the surface of the Ir coating was relative rough. The coating was composed of the tapered crystallites [30]. During the deposition, the as-deposited atoms, clusters, and particles suffered from the bombardment of the hybrid plasma. Some small atom clusters and particles were prone to be sputtered out. The high concentration of the Ir ions in the boundary layer led to the agglomeration of the Ir atoms. The agglomerated clusters and the sputtered Ir particles were deposited to form tapered crystallites. The average size of the crystalline grain was about 1 μm, which was larger than that of the Ir–Zr coating. It was evident that the grains of the Ir–Zr coating decreased with addition of Zr element. Compared with the Ir–Zr coating, the Ir coating was rough, which was in line with the AFM images (Fig. 3).

Fig. 5 shows the SEM micrograph and the EDS spectrums of the cross section of the Ir–Zr coating. The thickness of the Ir–Zr coating was 5.0 μm. The Ir–Zr coating was composed of two distinct layers. In the outside layer, the thickness of the coating was 2.4 μm with microcracks and particle debris. The microcracks were confined to the coating without propagating into the Mo substrate. In the inner layer, the coating was continuous with a thickness of 2.6 μm. The coating and the substrate exhibited good adherence with no evidence of delamination. The elemental compositions of the Ir–Zr coating were composed of the Ir, Zr, Mo and O (Fig. 5b and c). In Fig. 6, the EDS spectrum of different areas from the interface to the surface of the coating was shown. The proportion of Ir fluctuated at first, then decreased gradually from 30.73(at.%, Fig. 5b) in the surface of the coating to 11.19(at.%, Fig. 5c) in the interface. The trend of Ir line showed the content was a gradient distribution. The Zr distribution experienced a slight decrease in the coating. Compared with the Zr line, the proportion of the Ir was lower, which was attributed to the design of the target. During the sputtering, the sputtering rate of the Ir was higher than that of the Zr, therefore, the content of Ir had a great change while the Zr experienced a slight trend. The content of Mo increased marginally in the coating. It could be concluded that Mo atoms sputtered out the surface and diffused into the coating at the high temperature, which was consistent with the XRD pattern (Fig. 3). It was found that the O element decreased gradually with the increase of the coating thickness. It was known that some cracks and fragments were formed in the coating due to the formation of the oxide ceramics phase.

Fig. 7 shows the schematic formation process of the gradient layer. The elemental Zr content was the highest before the deposition because of the design of the alloy target. Along with the bombardment of Ar^+, the Ir and Zr were continuously deposited and sputtered out on the surface of Mo substrate (Fig. 7a). With the deposition, the Zr element declined steadily, consequently some Ir element could be gradually exposed from where Zr atoms had

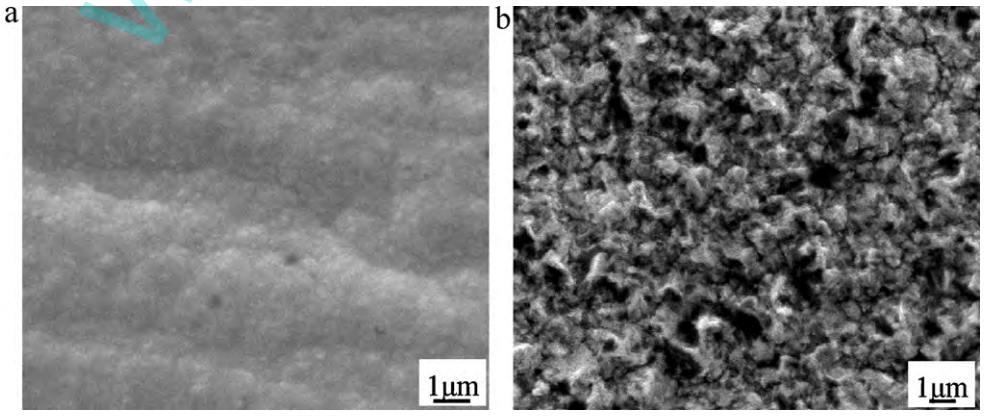

Fig. 4. SEM micrographs of the surface of the (a) Ir–Zr coating and (b) Ir coating.

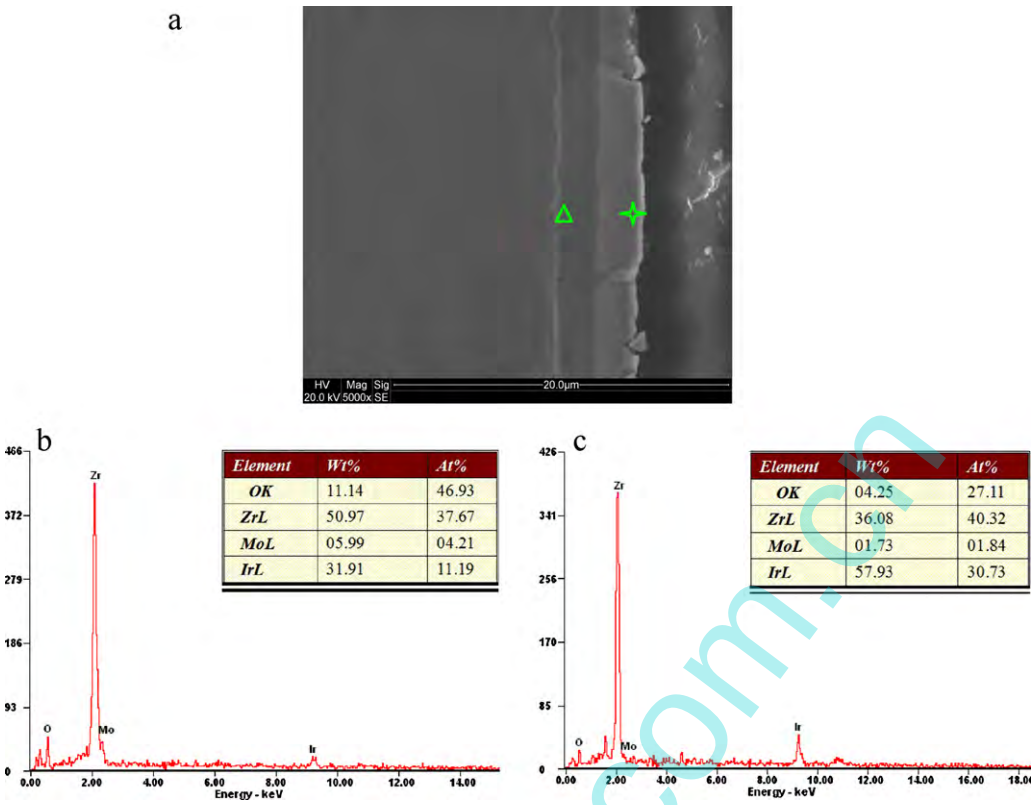

Fig. 5. SEM micrograph and EDS spectrums of cross section of the coating: (a) SEM photograph, (b) "✧" dot, and (c) "△" dot.

been covered. This also meant that the proportion of Ir on the target increased consistently. Besides, the Ir and Zr atoms diffused into the substrate at high temperatures, at the same time, the Mo atoms also diffused into the coating (Fig. 7b). The percentage of the coating elements changed constantly. Finally, the gradient layer with Zr and Ir concentration distributed was formed (Fig. 7c).

3.3. Adhesive property

Fig. 8 displays the SEM micrographs and scratch test pattern of the scratched coating. Some cracks occurred inside the scratch track without extensive chipping. From the amplificatory microstructure in the left corner of Fig. 8a, the relative curved cracks extended to the edges of the scratch track. Brittleness in polycrystalline Ir was intrinsic, and was not related to impurity [31]. From the SEM micrograph in the right corner of Fig. 8a, some microcracks occurred and the white areas showed poor adhesion. The adhesive force of the Ir–Zr coating was 15 N (see Fig. 8b). A general rule of thumb

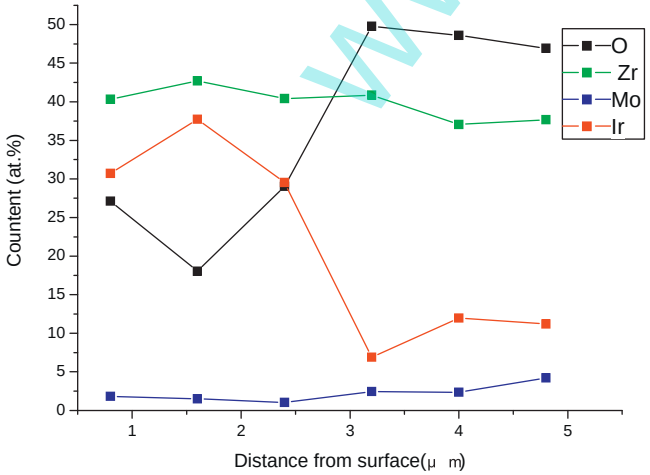

Fig. 6. Composition analysis of EDS spectrum of the coating.

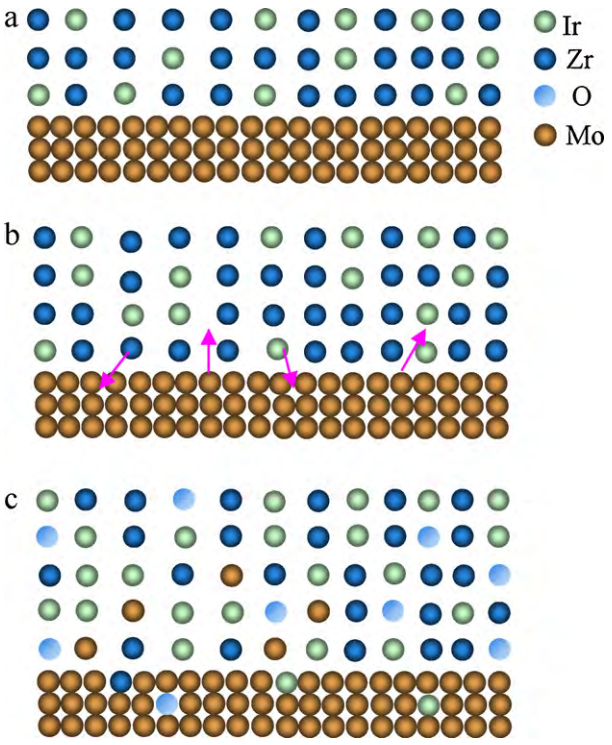

Fig. 7. Schematic formation process of the gradient layer growth: (a) beginning, (b) middle, and (c) last.

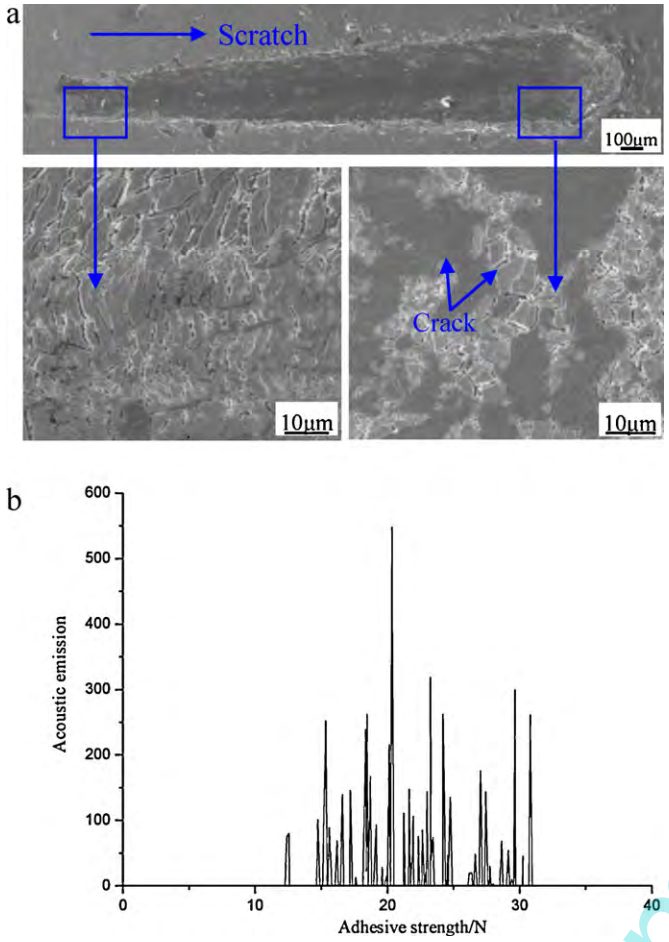

Fig. 8. SEM micrographs and scratch test pattern of the Ir–Zr coating: (a) SEM micrographs and (b) scratch test pattern.

says [32] that a critical load of 30 N in scratch testing with a Rockwell C diamond tip is generally sufficient for tooling applications. Therefore, the Ir–Zr coating adhered weakly to the substrate due to the formation of the brittle oxide ZrO_2 phase on the surface of the coating.

4. Conclusions

(1) Ir–Zr gradient coating was successfully obtained on the surface of Mo substrate by double glow plasma. The Ir–Zr coating was generally dense and homogeneous. The Ir–Zr coating with the thickness of 5.0 μm was composed of two layers. The interface between the coating and the substrate exhibited no delamination.

(2) The roughness values of the Ir–Zr coating was 19.3 nm with the grain size of 100 nm. Due to the addition of Zr in the coating and the formation of the ZrO_2 phase, the Ir–Zr coating had much finer grain structures as compared with the Ir coating under the same experiment conditions. Hence, the decrease of the roughness value in the Ir–Zr coating was due to the grain size refinement.

(3) A model has been made to explain the formation process of the gradient layer growth. The percentage of the coating elements were changed constantly during the deposition. Lastly, the gradient layer with Zr and Ir concentration distributed was formed.

(4) The adhesive force of the Ir–Zr coating was about 15 N. The Ir–Zr coating adhered weakly to the substrate due to the formation of the brittle oxide ZrO_2 phase on the surface of the coating. In the following investigation, we need to keep superhigh vacuum condition stopping the penetration of the oxygen.

Acknowledgments

This work has been supported by Funding for Outstanding Doctoral Dissertation in NUAA (BCXJ11-09) and Funding of Jiangsu Innovation Program for Graduate Education (CXLX11_0207).

References

[1] J.M. Wang, Z.W. Zhang, Z.H. Xu, X. Lin, W.P. Wu, Z.F. Chen, Oxidation of double glow plasma discharge coatings of iridium on molybdenum for liquid fuelled rocket motor casings, Corros. Eng. Sci. Technol. 46 (2011) 732–736.
[2] S.S. Brenner, Catastrophic oxidation of some molybdenum-containing alloys, J. Electrochem. Soc. 102 (1995) 16–21.
[3] R.W. Bartlett, Molybdenum oxidation kinetics at high temperature, J. Electrochem. Soc. 113 (1964) 744–746.
[4] J. Hagen, F. Burmeister, A. Fromm, P. Manns, G. Kleer, Iridium coatings with titanium sub-layer deposited by RF magnetron sputtering: mechanical properties and contact behavior with RoHS-compliant glass melt, Plasma Process Polym. 6 (S1) (2009) S678–S683.
[5] Y. Liu, C.T. Liu, L. Heatherly, E.P. George, Effects of alloying elements on dendritic segregation in iridium alloys, J. Alloys Compd. 459 (2008) 130–134.
[6] Y. Yamabe-Mitarai, Y. Gu, C. Huang, R. Völkl, H. Harada, Platinum-group-metal-based intermetallics as high-temperature structural materials, JOM 56 (9) (2004) 34–39.
[7] Y. Li, J.A. Woollam, Optical modeling of iridium thin film erosion under oxygen plasma exposure, J. Vac. Sci. Technol. A 22 (5) (2004) 2177–2181.
[8] K. Mumtaz, J. Echigoya, H. Enoki, T. Hirai, Y. Shindo, Annealing of aluminium oxide coatings on iridium-coated isotropic graphite at high temperature in argon atmosphere, J. Alloys Compd. 209 (1994) 279–283.
[9] M.R. Richards, Process development for IrAl coated SiC–C functionally graded material for the oxidation protection of graphite, PhD Thesis, University of Washington, 1996.
[10] Y. Yamabe-Mitari, Y. Ro, T. Maruko, H. Harada, Microstructure dependence of strength of Ir-base refractory superalloys, Intermetallics 7 (1999) 49–58.
[11] K. Kamiya, H. Murakami, Characterization of an Ir–Hf alloy coating as a bond coat material, J. Jpn. Inst. Met. 69 (2005) 73–79.
[12] A. Suzuki, Y. Wu, A. Yamaguchi, H. Murakami, C.M.F. Rae, Oxidation behavior of Pt–Ir modified aluminized coatings on Ni-base single crystal superalloy TMS-82+, Oxid. Met. 68 (2007) 53–64.
[13] P. Kuppusami, H. Murakami, T. Ohmura, Microstructure and mechanical properties of Ir–Ta coatings on nickel-base single-crystal superalloy TMS-75, J. Vac. Sci. Technol. A 22 (2004) 1208–1217.
[14] S.F. Tseng, C.T. Lee, K.C. Huang, D. y. Chiang, C.Y. Huang, C.P. Chou, Mechanical Properties of Pt–Ir and Ni–Ir binary alloys for glass-molding dies coating, J. Nanosci. Nanotechnol. 11 (2011) 1–7.
[15] F. Wu, H. Murakami, A. Suzuki, Development of an iridium–tantalum modified aluminide coating as a diffusion barrier on nickel-base single crystal superalloy TMS-75, Surf. Coat. Technol. 168 (2003) 62–69.
[16] K. Kamiya, H. Murakami, Characterization of an Ir–Hf alloy coating as a bond coat material, J. Jpn. Inst. Met. 69 (1) (2005) 73–79 (in Japanese).
[17] S.F. Tseng, W.T. Hsiao, K.C. Huanga, M.F. Chenc, C.T. Leea, C.P. Choub, Characteristics of Ni–Ir and Pt–Ir hard coatings surface treated by pulsed Nd:YAG laser, Surf. Coat. Technol. 205 (7) (2010) 1979–1984.
[18] T. Hirano, K. Wakashima, Mathematical modeling and design, MRS Bull. 20 (1995) 40.
[19] S. Suresh, Graded materials for resistance to contact deformation and damage, Science 292 (2001) 2447.
[20] W.P. Wu, Z.F. Chen, H. Cheng, L.B. Wang, Y. Zhang, Tungsten and iridium multilayered structure by DGP as ablation-resistance coatings for graphite, Appl. Surf. Sci. 257 (2011) 7295–7304.
[21] W.P. Wu, Z.F. Chen, X. Lin, B.B. Li, X.N. Cong, Effects of bias voltage and gas pressure on orientation and microstructure of iridium coating by double glow plasma, Vacuum 86 (2011) 429–437.
[22] Y. Zhang, Z.F. Chen, L.B. Wang, B. Yan, C. Li, D. Fang, Phase and microstructure of tungsten coating on C/C composite prepared by double-glow plasma, Fusion Eng. Des. 84 (1) (2009) 15–18.
[23] L.B. Wang, Z.F. Chen, Y. Zhang, W.P. Wu, Ir coating prepared on Nb substrate by double glow plasma, Int. J. Refract. Met. Hard Mater. 27 (2009) 590–594.
[24] Y. Ritterhaus, T. Hur'yeva, M. Lisker, E.P. Burte, Iridium thin films deposited by liquid delivery MOCVD using Ir(EtCp)(1,5-COD) with toluene solvent, Chem. Vap. Deposition 13 (12) (2007) 698–704.
[25] Z.F. Chen, W.P. Wu, L.B. Wang, Y. Zhang, Microstructure and analytic equation of conical aggregate in iridium coating prepared by double glow plasma, Surf. Eng. 27 (4) (2011) 242–245.
[26] M.A. El Khakani, M. Chaker, B. Le Drogoff, Iridium thin films deposited by radiofrequency magnetron sputtering, J. Vac. Sci. Technol. A 16 (1998) 885–888.

[27] W.P. Wu, X. Lin, Z.F. Chen, Z. Chen, X.N. Cong, T.Z. Xu, J.L. Qiu, Microstructural characterization and mechanical property of iridium coating produced by double glow plasma, Plasma Chem. Plasma Process. 31 (3) (2011) 465–475.
[28] Y.S. Gong, C.B. Wang, Q. Shen, L.M. Zhang, Effect of annealing on thermal stability and morphology of pulsed laser deposited Ir thin films, Appl. Surf. Sci. 254 (13) (2008) 3921–3924.
[29] N.V. Gelfond, N.B. Morozova, I.K. Igumenov, E.S. Filatov, S.A. Gromilov, Yu V. Shubin, R.I. Kvon, V.S. Danilovich, Structure of Ir and Ir–Al_2O_3 coatings obtained by chemical vapor deposition in the presence of oxygen, J. Struct. Chem. 51 (2010) 82–91.
[30] L.B. Wang, Z.F. Chen, P.Z. Zhang, W.P. Wu, Y. Zhang, Ir coating prepared on Mo substrate by double glow plasma, J. Coat. Technol. Res. 6 (4) (2009) 517–522.
[31] M.J. Cawkwell1, D. Nguyen-Manh, C. Woodward, D.G. Pettifor, V. Vitek, Origin of brittle cleavage in Iridium, Science 309 (2005) 1059–1062.
[32] S. Hogmark, S. Jacobson, M. Larsson, Design and evaluation of tribological coatings, Wear 246 (2000) 20–33.